Quantifying the optical properties and chromophore concentrations of turbid media using polarization sensitive hyperspectral imaging: optical phantom studies

Fartash Vasefi [a], Rolf Saager [b], Anthony J. Durkin [b], Nicholas MacKinnon [a], Eugene Gussakovsky [a], Robert Chave [a], Daniel L. Farkas [a, c,*]

[a] Spectral Molecular Imaging Inc., 250 N. Robertson Blvd, Beverly Hills, CA, USA 90211

[b] Beckman Laser Institute and Medical Clinic, University of California, Irvine, CA

[c] Department of Biomedical Engineering, University of Southern California, Los Angeles, CA, USA 90089

*(Corresponding author: dlfarkas@gmail.com)

ABSTRACT

We present a polarization-sensitive hyperspectral imaging system (SkinSpect) that employs a spectrally-programmable light source in the visible and NIR domains. Multiple tissue-mimicking phantoms were fabricated to mimic the optical properties of normal skin as well as pigmented light and dark moles. The phantoms consist of titanium dioxide and a mixture of coffee, red food dye, and naphthol green as the scattering and the three absorptive agents in a polydimethylsiloxane (PDMS) base. Phantoms were produced with both smooth and rough textured surfaces and tested using Spatial Frequency Domain Imaging (SFDI) and Spatially Modulated Quantitative Spectroscopy (SMoQS) for homogeneity as well as determining absorption and scattering variance, respectively. The reflectance spectral images were also recorded using the SkinSpect research prototype; the spectral signatures of the phantoms were calculated using a two-flux single-layer Kubelka-Munk model and non-negative least square fitting routine was applied to extract the relative concentrations of the individual phantom components.

Keywords: hyperspectral imaging, melanoma, multi-mode dermoscope, skin tissue optics, optical tissue phantom

1. INTRODUCTION

Development of biomimetic skin tissue phantoms provides an opportunity to validate new optical medical imaging tools and technologies under controlled conditions. The phantoms can be fabricated under closely controlled conditions and used for system calibration since they consist of pre-defined concentrations of individual components with targeted absorption and scattering levels [1][2][3][4]. In addition to optical properties, other tissue phantom characteristics such as durability, uniformity, mechanical behavior, reproducibility, and three-dimensional structure become important to consider depending on the targeted imaging modalities [5]. Recent attempts to mimic the epidermis and dermis layer thickness and surface geometry, combined with different absorption or scattering properties, were carried out with multilayer skin phantoms. These used fabrication methods such as spin coating to provide desired thickness layers up to ~ 100 µm [6]. Another approach employed a two-photon absorption microstereolithography system to fabricate complex microstructures, leading to more accurate mimicking of the papillary dermis structure [7].

Early phantoms were based on hydrogels (such as agar and gelatin). Although they are compatible with organic and non-organic additives as optical scatterers and/or absorbers, they suffer from low durability and rigidity at room temperature. Alternatively, the use of polydimethylsiloxane (PDMS) phantoms with titanium dioxide (TiO2) as the primary scattering agent has been detailed elsewhere [8]; these phantoms often require inorganic dyes (such as india ink) to provide the absorption characteristics. The greatest appeal of these phantoms is that they can be fabricated over a large range of optical properties and are stable over long periods of time (years); however, it is challenging to produce PDMS phantoms that can mimic the spectral content of skin over wide spectral ranges (visible and near infrared). Recently, researchers at the Beckman Laser Institute have proposed a method to incorporate coffee into PDMS phantoms to approximate the absorption characteristics of melanin [9].

In this paper, we first describe the polarization-sensitive hyperspectral imaging system (SkinSpect, SMI Inc.) components and the image data that it provides for our investigation in this phantom study. Since one of the main goals

Imaging, Manipulation, and Analysis of Biomolecules, Cells, and Tissues XI, edited by Daniel L. Farkas, Dan V. Nicolau, Robert C. Leif, Proc. of SPIE Vol. 8587, 85870Z
 · doi: 10.1117/12.2005371

of the system is to spectrally decompose tissue chromophores in skin, in this investigation we constructed simplified homogeneous tissue-simulating phantoms with three dyes that mimic optical properties of skin absorption with different melanin concentrations. The tissue phantom properties, such as absorption and scattering, were characterized using two spatial frequency domain imaging (SFDI) systems. Finally, the phantoms were tested using our prototype polarization sensitive hyperspectral imaging system. The spectral images were analyzed using a Kubelka-Munk model and linear least square fitting algorithm to extract the relative individual absorber dye concentrations.

2. METHODS

2.1 SkinSpect System overview

We developed a research prototype of the SkinSpect (SMI Inc.) having hyperspectral and polarization control capabilities along with software that was designed to use the extended functionality of this spectral imaging instrument in the measurement of skin lesions. As shown in Figure 1, the system consisted of a console and a handpiece probe. The console chassis housed a spectrally tunable illumination source along with a UNIX-based computer to control handpiece illumination, data acquisition, image processing, archiving, and data transmission. Additionally a touch-screen Windows-based computer was employed in the same console to create an intuitive, ergonomic interface to manage both instrument operation and patient records. The SkinSpect console employed a spectrally programmed digital light source which incorporated a OneLight Spectra system and additional sources. These sources included a Xenon arc lamp, and two supplemental LEDs at 385 nm and 455 nm. The handpiece contained two cameras mounted on a common frame; a beam splitter; and fiberoptic guides to direct light from the external illumination sources, as well as a tube that maintained the camera-illumination assembly at the correct focal depth to the tissue surface and excludes stray light. A linear polarizer was positioned in front of the fiber optics so that only linearly polarized light illuminated the tissue surface. Each of the two cameras had a polarization filter oriented at zero and 90 degrees, respectively, relative to the illumination polarizer. A single scan captured two images of an area of skin about 11 mm × 16 mm in size in both parallel and cross polarizations.

The handpiece can easily be positioned anywhere on the patient's body for a complete skin survey. The system operated in red, blue, green (RGB), fluorescence, and hyperspectral reflectance modes when activated by a single switch on the handpiece. Data acquisition was done by sequential imaging of the subject at the following illumination wavelengths: blue 452 nm, green 527 nm, and red 592 nm for an RGB image); 385 nm for fluorescence excitation; and sequential illumination of 30 wavelength bands from visible to the near infrared range. The 30 wavelength bands had 22 nm FWHM bandwidth and spanned a range from 497 nm to 945 nm at 15 nm wavelength intervals. The system software provided automatic data acquisition under control of an operator and automated calibration to confirm system accuracy on each data acquisition.

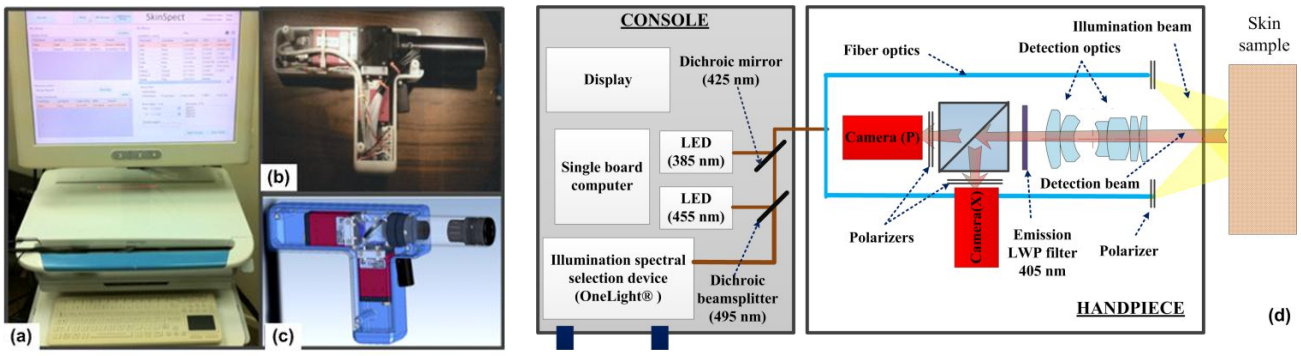

Figure 1 (a) The SkinSpect™ research prototype and the (b) handpiece module; (c) the CAD design of handpiece module; (d) Block diagram of SkinSpect™ research prototype system.

In the RGB mode, the primary illumination spectral selection device (OneLight Inc., Vancouver, BC) generated red and green illumination in 592 nm and 527 nm wavelengths and 50 nm FWHM bandwidth. Blue illumination was generated by an LED system at 455 nm. Dichroic beamsplitter (495 nm) located in the console optical bench was used to combine all three colors of illumination within a single beam path to the sample. The combined RGB image in both parallel and cross polarization modes yielded an instantaneous image of the scanned field of view. In the fluorescence mode, a 385 nm LED light source was used to excite autofluorescence in the skin. A second dichroic mirror (425 nm) merged the

excitation illumination into to the illumination path. The emission long pass filter in the detection path (cut-off wavelength = 405 nm) allowed only the emitted photons from autofluorescence to reach each individual camera.

At the beginning of the scanning session, the system was calibrated by scanning a high-reflectance white calibration target (e.g. Spectralon) to correct the illumination inhomogeneity; to adjust exposure time for each spectral band in order to ensure an acceptable signal to noise ratio; to subtract the 'dark current' image, and to remove 'hot' or bad pixels from the data set.

Figure 2 shows a representation of SkinSpect data output after sequential image capturing. The output datacube contained RGB, fluorescence, and diffuse reflected images of the skin with a total field of view covering 11 mm × 16 mm on the skin. The minimum spatially resolvable line width detected by P and X cameras was 39.4 µm and 111 µm respectively which were derived by imaging 1951 USAF Wheel Pattern Resolution Test Targets.

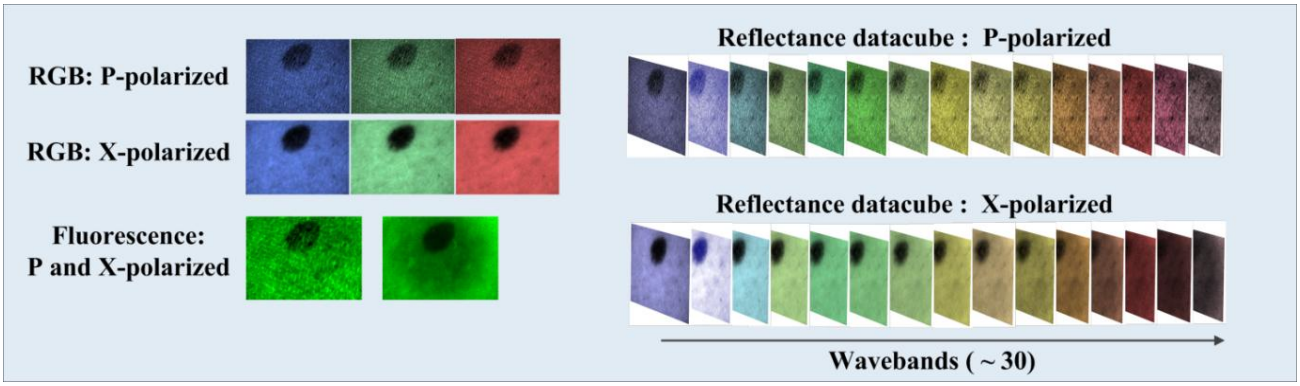

Figure 2 SkinSpect data output including RGB, fluorescence and hyperspectral diffused reflection images in parallel and cross polarization modes.

2.2 Optical phantom preparation

Three discrete concentrations of coffee (Albertson's Crystals Classic Roast, Distributor: SuperValu, New Eden, MN) were used to approximate the melanin pigmentation of 3 skin types [9]. Red food coloring dye (Food Color and Egg Dye, Essential Everyday, Distributor: SuperValu, New Eden, MN) and naphthol green B (Sigma-Aldrich, St. Louis, MO) where used to provide distinct spectral features in visible and near infrared wavelength ranges, while maintaining the overall optical property features of skin including high absorption in visible and low absorption in near infrared wavelengths. It is worth noting that that the red food dye absorber (with its slight blue shift of ~50 nm) provides a stable simulation of absorption behavior rather than actually mimics the α and β-band absorption of hemoglobin. Table 1 shows the respective combinations of dyes used to simulate each skin type as well as a fourth phantom that contained only the TiO_2 scatterer (Titanium Dioxide Powder, Atlantic Equipment Engineers, Bergenfield NJ), for reference. The basic spectra of the dyes used in skin phantoms are measured separately using a spectrophotometer system (see Figure 3c).

Table 1. Composition of tissue-mimicking phantoms.

Phantom	Coffee	Red food dye	Naphthol Green	Titanium Dioxide
P1: Skin-Type-I	0.4606g/200ml	4 drops/200ml	4.24mg/200ml	0.32g/200ml
P2: Skin-Type-II	1.842g/200ml	4 drops/200ml	4.24mg/200ml	0.32g/200ml
P3: Skin-Type-III	3.685g/200ml	4 drops/200ml	4.24mg/200ml	0.32g/200ml
TiO2	-	-	-	0.32g/200ml

As PDMS (Eager Plastics, Chicago, Il) is hydrophobic, all combinations of dyes were prepared in an alcohol based solution and independently verified by spectrophotometer for their absorption characteristics in this environment. The dyes were mixed with the raw PDMS and the TiO2 was mixed with the curing agent and sonicated for 1 hour to ensure even dispersal of the TiO2 particles [8]. Once the raw PDMS was mixed with the curing agent, it was poured into

rectangular forms and placed in a vacuum chamber overnight, to ensure that all air bubbles introduced in the mixing have been removed. To create a textured surface, 320-grit sandpaper was placed in the bottom of each form, while the top was allowed to cure smooth. Figure 3a shows the three phantom material with absorbers but no scatterer in cuvettes suitable for spectral measurement. The cuvettes used have a 3 mm optical path length at the bottom and a 1 cm optical path length at the top. As shown in Figure 3b, three skin type phantoms were fabricated with dimensions of 10 cm ×10 cm and with thickness > 2 cm. The TiO2 phantom dimensions are 7.5 cm ×7.5 cm × 1 cm. All phantoms are significantly larger than the measurement field in order to minimize boundary effects.

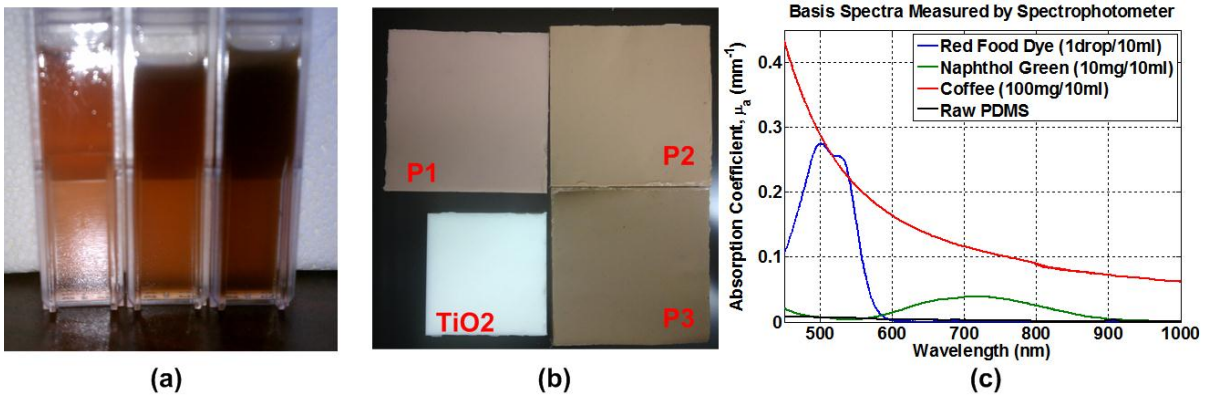

Figure 3. (a) Three skin-type phantoms in non-scattering PDMS base cuvettes (top area is 1cm pathlength, the bottom area is 3 mm pathlength). (b) Picture of three skin phantoms (roughened surface) with the TiO2 phantom. (c) Basic absorption of individual dye used in skin phantom by Shimadzu UV 3600 spectrophotometer.

2.3 Optical phantom characterization

The quantification and characterization of the optical properties of these phantoms were performed by two instruments based on the principles of spatial frequency domain imaging (SFDI) [10]. The first instrument, referred to as MI2, employs a wide field imaging approach to validate the homogeneity of the fabricated phantoms. This instrument uses a CCD with a liquid crystal tunable filter (LCTF) to image the reflectance from the phantoms, while the phantoms are illuminated by projected illumination pattern of multiple spatial frequencies, at 17 discrete wavelengths (ranging from 650-970nm). While this measurement was limited to the near infrared range, this imaging modality provided detailed spatial information to characterize the homogeneity of the optical properties of the phantoms.

SMoQS is a point spectroscopy system with high spectral resolution (~1nm) that also exploits SFDI methods, but spans both visible and near infrared wavelength ranges [11] [12]. This technique was used to measure these phantoms in three random regions of interest (ROIs) to determine the quantitative optical properties (i.e. absorption and reduced scattering coefficients) from 450 to 950nm. These measurements also match the optical properties measured by MI2 in the near infrared as a means to cross-validate these results and infer the tolerances given by MI2 regarding the variance in homogeneity within these phantoms.

2.4 Spectral decomposition algorithm

As a proof of concept, we used a homogenous structure with an assumption of isotropically absorbing and scattering layer of infinite thickness, we used two-flux Kubelka-Munk (KM) based model [13] to extract the relative phantom dye concentrations.

$$\frac{K}{S} = \frac{\left(1 - R(\lambda)\right)^2}{2R(\lambda)}$$

where $R(\lambda)$ is normalized reflectance spectra which calculated from intensity of phantom-reflected light by the intensity of light reflected from the white Spectralon. K and S are the total absorption and scattering contribution of phantom dyes. By assuming that the additivity of the phantom dye absorbers is valid, we can assume:

$$K = C_1\varepsilon_1 + C_2\varepsilon_2 + C_3\varepsilon_3 + \ldots$$

$$S = a + b\lambda^{-m}$$

where C and ε are the relative concentration and extinction coefficient of each phantom dye. We employed a three dye system of coffee, naphthol green and red food dye as the major dye contributions in the phantoms. The phantom scattering was extracted as a power function from the SMoQS system. The predicted K/S spectrum was fitted to the measured K/S spectrum by a MATLAB (the Mathworks, Natick, MA) standard non-negative least square (NNLS) fitting function to extract the relative concentration of each dye in the phantom being measured.

3. RESULTS AND DISCUSSION

Figure 4 summarizes the spatial variances and spectral content of the fabricated phantoms' optical properties (absorption and scattering coefficients) as determined by the MI2 system. Phantoms corresponding to skin types I, II, and III (with different melanin concentrations), respectively, are shown in Figure 4 (a-c). Figure 4 (d) shows results from the phantom that contained TiO2 only (no dyes). The relative spatial variances in absorption for these phantoms were 1.5, 1.3, 4.7 and 7%, respectively. The high absorption variance in the TiO2 phantom may be due to its substantially lower absorption. The relative spatial variances in reduced scattering were 1.0, 1.7, 4.3, and 1.1% respectively (here, the high concentration of coffee in (c) resulted in undissolved granules that also contributed to scattering).

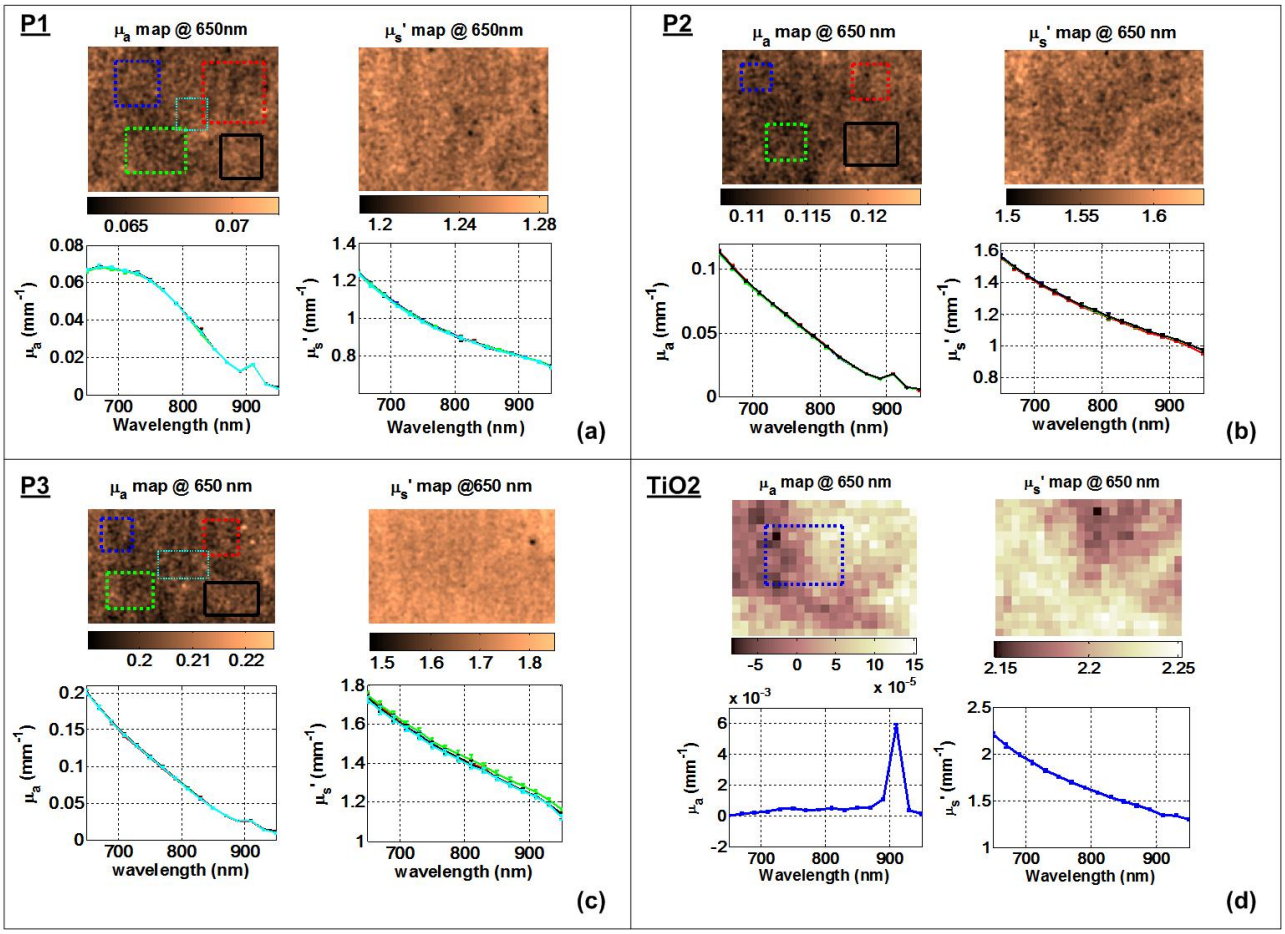

Figure 4. Summary of spatial and spectral optical properties as characterized by MI2 system.

Figure 5 summarizes the results from three separate measurements for each phantom using the SMoQS instrument (with ~1nm spectral resolution). Measurements of optical properties (absorption and scattering coefficients) of phantoms corresponding to skin types I, II, and III, respectively, are shown in Figure 5 (a-c). Figure 5 (d) shows results for the phantom that contained TiO_2 only (no dyes). The absorption spectrum features of the red food dye and the naphthol green become less evident on the total absorption spectrum as the coffee concentration increases. The absorption decay slope around 550 nm is steeper in the phantom corresponding to skin type I and decreases in the skin type II and III phantoms. This is analogous to the changes in the absorption spectrum of normal skin compared to the absorption

spectrum of highly pigmented skin with higher melanin concentrations, although the absorption drop in skin usually occurs at about 600 nm. This is due to the 50 nm blue shift in the absorption response of red food dye compared to that of hemoglobin.

Although the coffee concentration in skin type II and III are four and eight times that used for skin type I, respectively, with the same red food dye and naphthol green concentration, the increase in absorption coefficient does not follow the same rate as the dye concentrations. This may also be due to undissolved coffee granules in the phantoms with higher coffee concentration, and we are further exploring this issue.

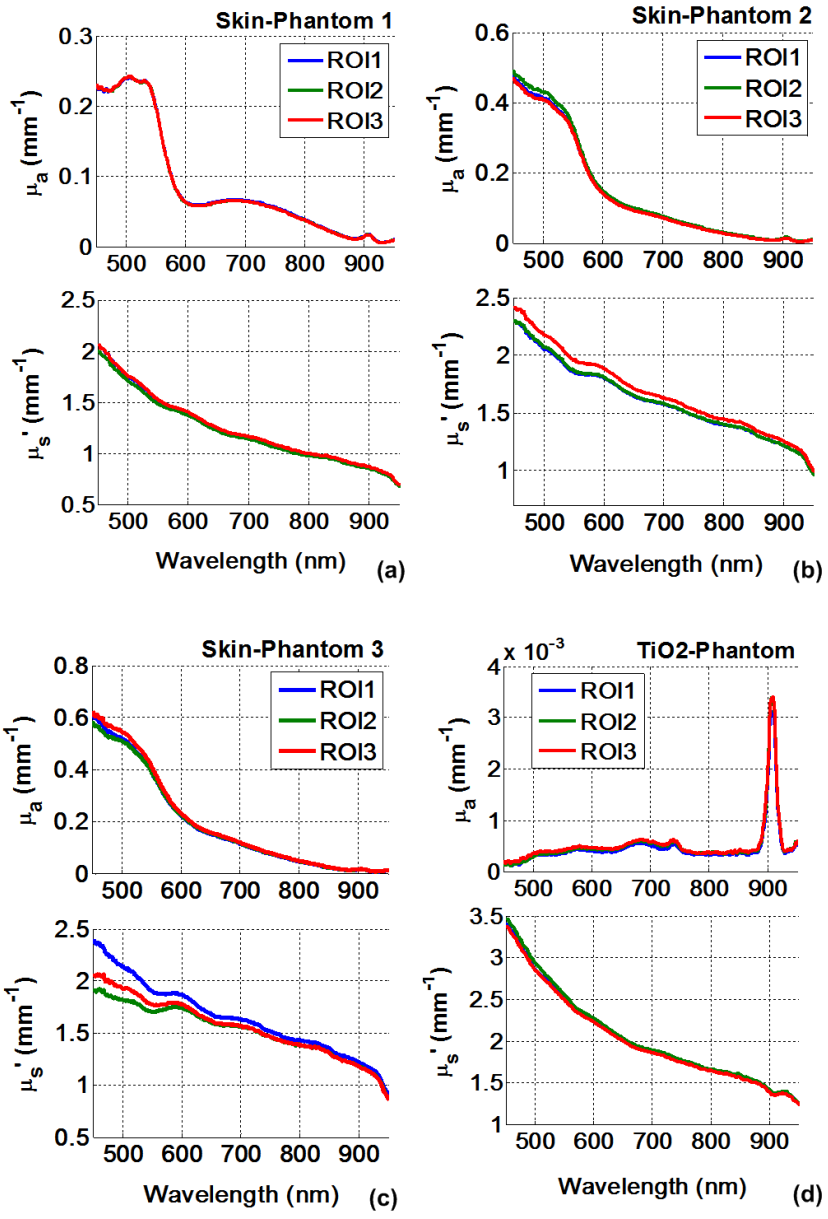

Figure 5. Summary of the visible and near infrared optical properties of the phantoms as characterized by SMoQS system

To spectrally decompose the relative concentrations of the dyes in the phantoms, we have used a single step non-negative least square fitting function based on the Kubelka-Munk model described in the method section above. Figure 6a shows the KM spectral response calculated from SkinSpect diffuse reflectance spectral images of three skin

mimicking phantoms. Figure 6b shows the same phantoms measured with a high-resolution point spectroscopy system (SMoQS). The reflectance spectra acquired using the SkinSpect were normalized using Spectralon (98% white) (Labsphere, North Sutton, NH) as reference to correct for the instrument response functions while in the SMoQS system the reference target is a PDMS based calibration reference phantom, as described in [12]. This difference in calibration procedures leads to some differences in the KM spectral signature at wavelengths longer than 800 nm. In addition, the KM spectra in SkinSpect and the point spectroscopy system were obtained at different spectral resolutions (~ 22 nm compared to ~1nm) which may be another reason that the spectral responses in Figure 6a and Figure 6b do not perfectly match.

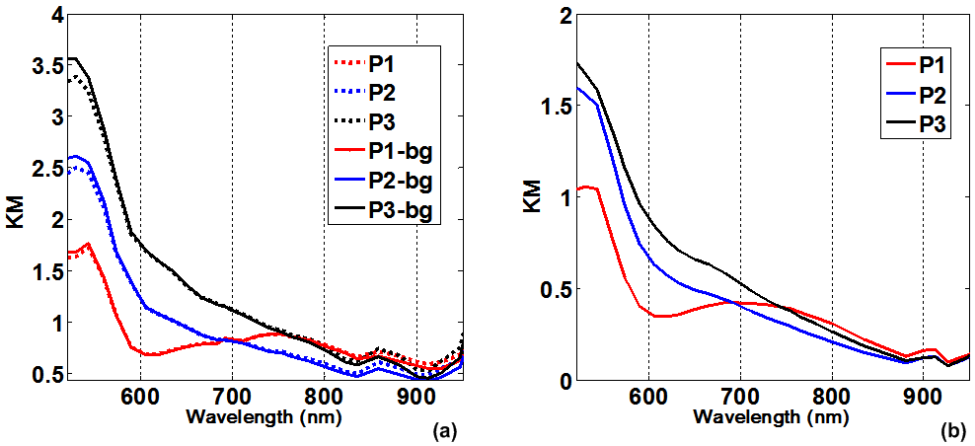

Figure 6. The Kubelka-Munk spectra measured using (a) SkinSpect system (dashed lines are the KM spectra with background illumination correction) and (b) high resolution point spectroscopy system (SMoQS). P1, P2, and P3 represent the spectra measured from phantoms mimicking skin type I, II, and III (different melanin concentrations).

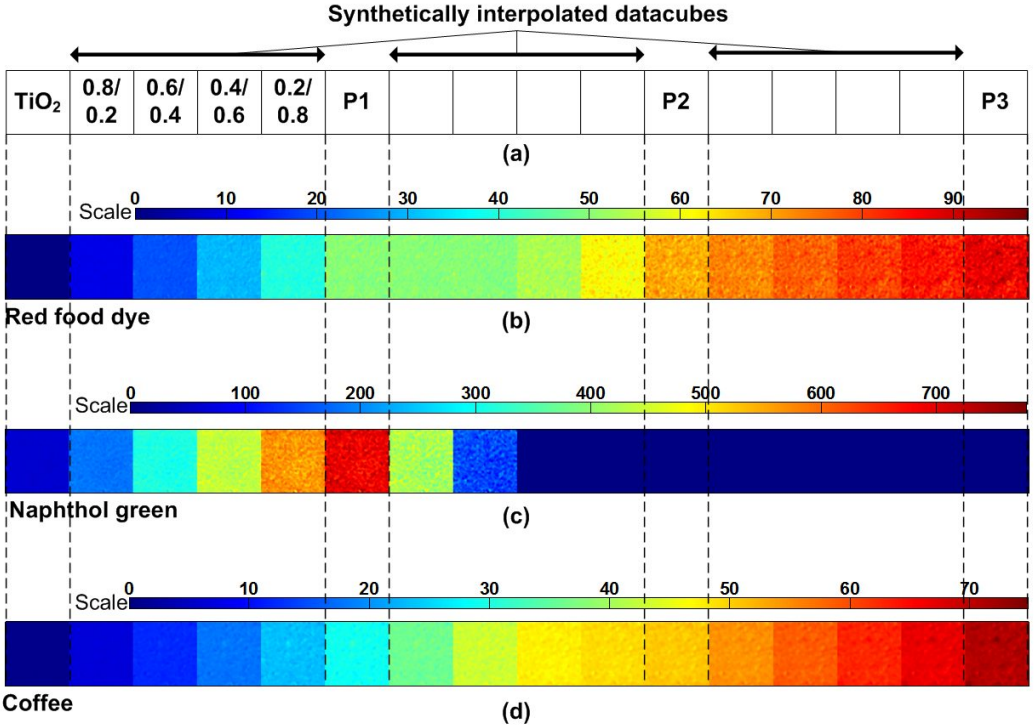

Figure 7. The spectral decomposition of Kubelka-Munk spectra measured by SkinSpect system for the phantoms as well as the synthetically added data. (Scale bars are the relative concentrations of each dye in the phantoms)

As described in the methods, SkinSpect is using a OneLight Spectra instrument to digitally select the desired spectral illumination. The OneLight Spectra uses a MEMS based spatial light modulator, commonly called a DLP (digital light processor) chip, which determines the specific spectrum that will be selected for illumination, by turning on and off tiny mirrors [14]. However, even when all these micro mirrors are off, straight light from the edges of the micro mirrors can create an unwanted background illumination (relative magnitude of less than 0.1 %) which must be subtracted. This background artifact increases for longer camera exposures. Figure 6 shows the KM spectral data with background light correction (solid lines) compared to the spectral data without correction (dashed lines). By comparing the Figure 6a to Figure 6b, we observe the background corrected KM spectra more closely resemble our reference point spectroscopy measurements, especially in 500-600nm wavelength ranges.

We decided to test the numerical fitting tolerances of the proposed Kubelka-Munk algorithm using the non-negative least square fitting function. Due to the limited number of phantoms available, we created synthetic combinations of KM datacubes linearly interpolated between the datacubes from the four fabricated phantom measurements. A total of 12 interpolated datacubes, four between each original phantom, were created to help understand where the proposed spectral decomposition algorithm would become numerically unreliable due to relative change in each dye concentrations. We used 16 wavebands from 543 – 783 nm with the intervals of ~ 15 nm.

Figure 7a is a diagram showing how an array of 100 × 100 pixel images from each phantom as well as images from the interpolated datacubes were structured. Figure 7(b-d) shows the resulting spectral decomposition maps of relative concentrations of red food dye, naphthol green and coffee. As expected, the dyes' concentrations show an increase from the TiO_2 phantom to the phantom corresponding to skin type I. However from phantom 1 to phantom 3, we would expect that only the coffee concentration would increase and the naphthol green and red food dye would remain constant. In contrast, we observed overestimation of red food dye in phantom datacubes corresponding to skin types II and III. The overestimation error is analogous to the mis-estimation observed in pigmented skin due to crosstalk (spectral similarities) between deoxy hemoglobin and melanin. We believe the fabricated phantoms shows spectral cross talk behaviors similar to melanin and hemoglobin in the pigmented skin [15][16][17]. Therefore, they are good candidates for spectral decomposition algorithm development and validation.

4. CONCLUSIONS

Multiple PDMS-based homogenous tissue phantoms were fabricated to mimic the optical properties of normal skin as well as of pigmented light and dark moles. The phantoms consisted of titanium dioxide and a mixture of coffee, red food dye, and naphthol green as the scattering and the three absorptive agents in a solid matrix of PDMS. Spatial homogeneity and optical property variations (absorption and scattering coefficients) in different fields of view were validated using two spatial frequency-domain imaging systems. The diffuse reflectance intensity recorded in cross polarization mode was analyzed using a Kubelka-Munk formalism-based algorithm. The KM spectral data for the fabricated phantoms, in both SkinSpect and point spectroscopy system (SMoQS), were compared and analyzed. The KM spectral data were spectrally decomposed using a linear non-negative least square fitting function to extract relative concentrations of the individual phantom components.

5. ACKNOWLEDGEMENTS

This work was supported (D1969B1) by the Qualifying Therapeutic Discovery Program under the US Department of Health and Human Services Patent Protection and Affordable Care Act of 2010, and SMI corporate funds. We wish to thank Drs. B. Tromberg and E. Lindsley for useful discussions and advice. We wish to also thank the NIH, NSF and DoD for past funding that made this work possible. Dr. Saager and Dr. Durkin gratefully acknowledge funding support from P41EB015890 (A Biomedical Technology Resource) from NIH/NIBIB.

REFERENCES

[1] Pogue, B. W., and Patterson, M. S., "Review of tissue simulating phantoms for optical spectroscopy, imaging and dosimetry," J. Biomed. Opt. 11(4), 041102 (2006).
[2] Nordstrom, R. J., "Phantoms as standards in optical measurements," Proc. SPIE 7906, 79060H (2011)
[3] V. V. Tuchin, Tissue Optics: Light Scattering Methods and Instruments for Medical Diagnosis (SPIE, 2000).

[4] Vasefi, F., Najiminaini, M., Ng, E., Chamson-Reig, A., Kaminska, B., Brackstone, M., and Carson, J., "Transillumination hyperspectral imaging for histopathological examination of excised tissue," Journal of biomedical optics, 16(8), 086014-086014, (2011).
[5] Lamouche, G., Kennedy, B. F., Kennedy, K. M., Bisaillon, C. E., Curatolo, A., Campbell, G., Pazos, V., and Sampson, D. D., "Review of tissue simulating phantoms with controllable optical, mechanical and structural properties for use in optical coherence tomography," Biomed. Opt. Express 3, 1381-1398 (2012)
[6] Yu, B., Yo., B., Lee, J., and Jung, B., "Characterization of a solid optical tissue phantom fabricated by spin coating method: pilot study," Proc. SPIE 8229, 82290U-82290U8 (2012)
[7] Matcher, S. J., Geca, P., and Claeyssens, F., "Fabrication of a skin phantom for OCT imaging using two-photon abssortion microstereolithography" Proc. SPIE 8583 (2013) [2013 BiOS SPIE Photonics West Technical Summeries, p.313]
[8] Ayers, F., Grant, A., Kuo, D., Cuccia, D. J., and Durkin, A. J., "Fabrication and characterization of silicone-based tissue phantoms with tunable optical properties in the visible and near infrared domain," In Proc. SPIE, 6870, 687007, 687007-9, (2008).
[9] Saager, R. B., Kondru, C., Au, K., Sry, K., Ayers, F., and Durkin, A. J., "Multilayer silicone phantoms for the evaluation of quantitative optical techniques in skin imaging," In Proc. SPIE, 7567, 756706, (2010).
[10] Cuccia, D. J., Bevilacqua, F., Durkin, A. J., Ayers, F. R., and Tromberg, B. J., "Quantitation and mapping of tissue optical properties using modulated imaging," Journal of biomedical optics, 14(2), 024012-024012 (2009).
[11] Saager, R. B., Cuccia, D. J., & Durkin, A. J., "Determination of optical properties of turbid media spanning visible and near-infrared regimes via spatially modulated quantitative spectroscopy," Journal of biomedical optics, 15(1), 017012-017012 (2010).
[12] Saager, R. B., Truong, A., Cuccia, D. J., and Durkin, A. J., "Method for depth-resolved quantitation of optical properties in layered media using spatially modulated quantitative spectroscopy," Journal of biomedical optics, 16(7), 077002-077002 (2011).
[13] Klier, K., "Absorption and Scattering in Plane Parallel Turbid Media," J. Opt. Soc. Am. 62, 882-885 (1972)
[14] Application note- DLP contrast and stray light, http://www.onelightcorp.com (last access: February 2013)
[15] Kuzmina, I., Diebele, I., Jakovels, D., Spigulis, J., Valeine, L., Kapostinsh, J., and Berzina, A., "Towards noncontact skin melanoma selection by multispectral imaging analysis," J. Biomed. Opt., 16(6), 060502-060502-3 (2011).
[16] Nishidate I, Tanaka N, Kawase T, Maeda, T., Yuasa, T., Aizu, Y., Yuasa, T., Niizeki, K., "Noninvasive imaging of human skin hemodynamics using a digital red-green-blue camera," J. Biomed. Opt., 16(8), 086012-086012-14 (2011).
[17] MacKinnon, N. B., Vasefi, F., Gussakovsky, E., Bearman, G. H., Chave, R., Farkas, D. L., "In vivo skin chromophore mapping using a multimode imaging dermoscope (SkinSpec™)", Proc. SPIE 8587, Imaging, Manipulation, and Analysis of Biomolecules, Cells, and Tissues XI, 85870U (2013)